Dependence of the Reactivity of Acridine on Its Substituents: A Computational and Kinetic Study

Zbigniew Zawada,[a] Jaroslav Šebestík,[a] Martin Šafařík,[a] and Petr Bouř*[a]

Aromatic nucleophilic substitution on the C9 carbon of acridine plays an important role in multiple biological and medicinal applications. The rate of the key reaction is strongly dependent on the environment and acridine substituents. In this study, the factors influencing the reaction mechanism were studied theoretically and verified experimentally for simplified systems. Density functional theory was used for the computations. The activation energy of a model derivative was determined experimentally from a kinetic study. Also, the relative reactivities of selected compounds were verified by a competition experiment. The theoretical predictions correlate well with the observations. The computed reaction path confirms that the thiol group attacks the aromatic core activated by the nitrogen heteroatom and replaces halogen or amino substituents via a well-defined Meisenheimer transition state. The reaction barrier is strongly influenced by both the solvent and substituents on the aromatic system. A multistep mechanism is proposed for the reaction of aminoacridine in which the aqueous solvent participates in the reaction. Strong correlations between reaction energies and geometrical parameters were observed and can be used to rationalize the design of acridine drugs as well as to avoid lengthy computations of the transition states.

Introduction

The tricyclic aromatic acridine system (Scheme 1) exhibits its increased reactivity at the 9-position relative to the corresponding all-carbon arene due to the presence of the nitrogen heteroatom.[1] Acridine and its derivatives, such as 9-aminoacridines, are widely used in medicine and biochemistry as drugs and labeling agents.[2]
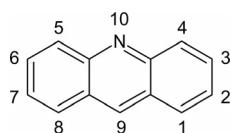
Scheme 1. Acridine and the atomic numbering pattern.

Acridine-based compounds have been considered, for example, for the treatment of protozoal infections, cancer, viral, and prion diseases. The covalent attachment of acridines can modulate the biological activity of peptides and proteins.[2a,2b,2d,3] Derivatives of 9-aminoacridine are used as efficient drugs;[2b,4] their anticancer activity is increased by their covalent binding to nucleic acids.[5] The quinacrine derivative is used, for example, in the treatment of rheumatic arthritis, Lupus erythrematosus, malaria, tapeworm infections, Chagas disease, and epilepsy.[4a,4b,6] Quinacrine inhibits the generation of the toxic isoform of the prion protein in an intoxicated cell culture.[4b] Bis-acridinylated compounds have also been tested for anti-prion activity.[4c,7] Finally, the 9-aminoacridine drug tacrine (9-amino-1,2,3,4-tetrahydroacridine) has been used in the treatment of Alzheimer's disease.[8]

The reactivity of acridines can be modified by their substituents. For instance, 9-amino substitution has been proposed to increase biological activity.[9] Acridines without a substituent at C9 are potent anticancer drugs.[10] Nevertheless, there are only a limited number of rules for predicting the reactivity of a particular derivative. The influence of acridine substituents on its reactivity has not been supported by a systematic theoretical analysis.

In this work, to enhance the future design of other biologically functional derivatives and to understand the function of this molecule on the atomic level, we have employed quantum chemical modeling. For a limited number of systems, the results have been verified experimentally. It appears that the reactivity of acridine can be modeled quite reliably and modeling confirms that the most probable reaction mechanism of the binding of acridine in organisms is aromatic nucleophilic substitution.[11] The influence of solvent was simulated by using the polarizable continuum dielectric model.

Although there are many possible mechanisms for the nucleophilic substitution of aromatic halides,[12] we have found the formation of the Meisenheimer complex as a

[a] Molecular Spectroscopy, Institute of Organic Chemistry and Biochemistry,
Flemingovo náměstí 2, 16610 Prague, Czech Republic
Fax: +420-220183578
E-mail: bour@uochb.cas.cz

WILEY ONLINE LIBRARY

transition state to be the most reasonable pathway for our systems. For example, radical mechanisms have been excluded due to the excess of mercaptans, which are efficient scavengers of free radicals. Moreover, calculated energy profiles along the reaction coordinate indicate that Meisenheimer's complex is the transition state (TS) of the rate-determining step rather than an intermediate.

Aromatic nucleophilic substitution is omnipresent in acridine chemistry, for example, in reactions with NH_2OH, $PhNHNH_2$, or thiols.[6c,11,13] The reactions strongly depend on temperature, pH, and the nucleophilicity of the attacking agent.[13a,14] To the best of our knowledge, the reactions have not been extensively investigated theoretically, except for single molecule energetics.[11,15]

Because of the significance for prion biochemistry, we have concentrated on the condensation reaction between acridine and the thiol group, which can take place on reduced disulfide linkages within the protein molecule. The reactivity and structure of a prion can potentially be influenced by the attachment of an acridine label. In particular, reduction and subsequent alkylation prevent the conversion of a prion into a protease resistant form.[16] An unperturbed disulfide linkage is important for a proper insertion of a prion into a membrane.[16b,16c]

First, activation barriers and reaction energies were calculated for a model pyridine system in which a chlorine atom was used as the leaving group. The computationally simplest SH^- nucleophile was used in most computations. For a limited number of systems, we verified that the reaction mechanism and relative energy ordering are the same for MeS^- and benzyl mercaptan (BM). Secondly, the optimal computational method (B3LYP/6-31+G**/CPCM) was then chosen for the whole acridine. This simplification enabled us to consistently compare more methods; months of CPU time would be needed for a TS computation of a larger system, even at a relatively low approximation level. The computational model also provides trends of reactivity that are in very good agreement with the kinetic control and competition experiments, which, clearly, could not be modeled in full.

The computation suggests a limited role of the aromatic acridine side-rings in the underlying reaction, which is located on the internal ring. The specific role of more distant acridine substituents (e.g., MeO, Cl, NO_2, and CF_3) on the reaction rate was investigated for a large set of acridine derivatives. The correlation between geometry and energy parameters provides a way to estimate reactivity without a laborious search for the transition state, perhaps also for more complicated acridine systems.

The activation energy was then estimated experimentally for a model system. For a larger set of acridine derivatives, relative reactivities obtained from a competition experiment are qualitatively compared with calculated activation energies. Finally, a multistep mechanism in an aqueous environment is proposed for the case in which chlorine at the 9-position of acridine is replaced by an amine and verified by computations of the intrinsic reaction coordinate. The computations suggest that the formation of the Mei-

senheimer complex during the aromatic nucleophilic substitution is also the rate-determining step in this case.

Results and Discussion

Energetics and Transition Complex of a Model Reaction

The validity of the methods was tested on the simplified reaction (1). The activation barrier, reaction energy, and selected geometry parameters, calculated at different levels of approximation, are summarized in Table 1. We can see that the reaction energies (ΔE) are relatively indifferent to the approximation used, whereas larger differences are apparent for the activation barriers (E^*). The barriers are also more influenced by the solvent environment. For water, their magnitudes are in the range 81–192 kJ/mol, whereas in vacuo, very low barriers were calculated by methods comprising electron correlation (DFT, MP2). The BPW91/6-31G** level could not be included because the computed "barrier" is negative, which implies that the transition state was not found.
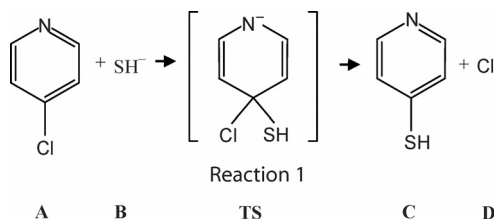

Reaction 1

Table 1. Calculated activation (E^*) and reaction (ΔE) energies for the model reaction (1) and selected distances (r) in the transition state (Figure 1).

	E^* [kJ/mol]	ΔE [kJ/mol]	r_{C-Cl} [Å]	r_{C-S} [Å]	r_{S-H} [Å]
Vacuum calculations					
HF/6-31G**	91	−107	1.837	2.251	1.331
MP2/6-31G**	1	−105	1.776	2.535	1.336
B3PW91/6-31G**	0	−97	1.824	2.444	1.348
B3LYP/6-31G**	4	−97	1.876	2.386	1.351
B3PW91/6-31++G**	12	−101	1.829	2.376	1.348
B3LYP/6-311++G**	16	−99	1.874	2.340	1.349
CPCM (H_2O)					
HF/6-31G**	192	−119	1.863	2.183	1.330
MP2/6-31G**	101	−117	1.862	2.183	1.333
B3LYP/6-31G**	106	−109	1.952	2.287	1.350
B3PW91/6-31++G**	101	−116	1.877	2.237	1.347
B3LYP/6-311++G**	105	−130	1.925	2.265	1.349
B3LYP/6-31+G**	122	−137	1.926	2.264	1.349
MP2/6-311++G2dp	81	−124	1.871	2.183	1.337

The CPCM results (lower part of Table 1) are more relevant to the usual experimental conditions and also more consistent for different levels of calculation. The sensitivity to the solvent is in accord with the observed dependence of acridine reactivity on the environment.[1,13a,14a] The HF method provides the highest activation barrier for both the in vacuo and CPCM calculations, which indicates the im-

portance of involving the correlation energy in the calculations. The MP2 results are quite close to those obtained by the DFT methods. The variation of the basis set causes a relatively minor change in energy, approximately within 10–20% for the basis sets examined. The B3LYP/6-31+G**/CPCM method was used for computation of the larger systems involving acridine described below as a compromise between speed and accuracy. It is reasonably fast and involves diffuse functions, at least on heavy atoms, which is presumably very important for a study of the reaction mechanism.

All the methods also predict a similar geometry for the activated complex (Figure 1, Table 1). The H–S–C and S–C–Cl angles are predicted to vary in the range of 83–95° by all models, and thus are not listed. The sulfur atom approaches the C4 atom from a direction approximately perpendicular to the aromatic ring and the system adopts a tetrahedral arrangement. Within the CPCM environment, the C–S bond becomes significantly shorter than determined by in vacuo calculations. Note also that consideration of the solvent leads to a reduction of the reaction energy. In more polar solvents the reaction is thus supposed to proceed more slowly than in vacuo, but with a higher reaction yield.
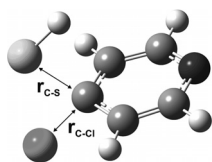

Figure 1. Geometry of the activated complex (B3LYP/6-311++G**/CPCM) in reaction (1).

Reactivity of Acridine Derivatives

At the B3LYP/6-31+G**/CPCM level we investigated the reactivity of the aminoacridine **6** and selected 9-chloroacridines (Figure 2). Protonated species were considered separately (e.g., **1** ≠ **5**) as they are treated as individual molecules in the calculations. The reaction energies calculated with the hydrogen sulfide anion and selected geometry pa-

rameters are summarized in Table 2. The 9-chloroacridines are clearly predicted to react faster than the 4-chloropyridine benchmark model. For the acridines, the activation energy is lowest for the protonated nitro analogue **1** (5 kJ/mol) and highest for the partially saturated compound **18**.

Table 2. Activation energies (E^*) and selected bond lengths in the reactants ($r_{C-Cl,react.}$) and transition states ($r_{C-Cl,TS}$, r_{C-S}, and r_{S-H}) for the acridine analogues summarized in Figure 2, as calculated at the B3LYP/6-31+G**/CPCM(H$_2$O) level.

System	E^* [kJ/mol]	$r_{C-Cl,react.}$ [Å]	$r_{C-Cl,TS}$ [Å]	r_{C-S} [Å]	r_{S-H} [Å]
4-Chloropyridine	122	1.757	1.926	2.264	1.349
1	5	1.726	1.732	3.102	1.352
2	18	1.733	1.753	2.748	1.351
3	20	1.732	1.755	2.717	1.351
4	32	1.739	1.766	2.623	1.350
5	52	1.749	1.789	2.451	1.350
6	59		–	2.583	1.350
7	62	1.751	1.801	2.380	1.350
8	69	1.752	1.819	2.311	1.349
9	71	1.753	1.820	2.318	1.350
10	72	1.750	1.821	2.358	1.349
11	74	1.754	1.823	2.305	1.350
12	76	1.754	1.829	2.293	1.349
13	79	1.755	1.833	2.287	1.349
14	81	1.752	1.830	2.294	1.348
15	86	1.757	1.846	2.259	1.349
16	88	1.757	1.851	2.249	1.349
17	96	1.759	1.869	2.233	1.349
18	116	1.764	1.959	2.261	1.350
3 (exp.)	35				

There is a low variance in the total reaction energies (from –118 kJ/mol for **18** to –136 kJ/mol for **1**, see Table S2 in the Supporting Information), slightly lower than for the pyridine model (–137 kJ/mol). The geometries of the transition states are also similar to those of pyridine.

When a methylamine group was attached to C9 instead of chlorine (compound **6**), a similar transition state was calculated in the rate-determining step. Acridine protonation (compounds **1–3** and **6**) leads to lower activation energies and thus speeds up the reaction in comparison with the corresponding unprotonated compounds. This is in agreement with the known behavior of acridine compounds.
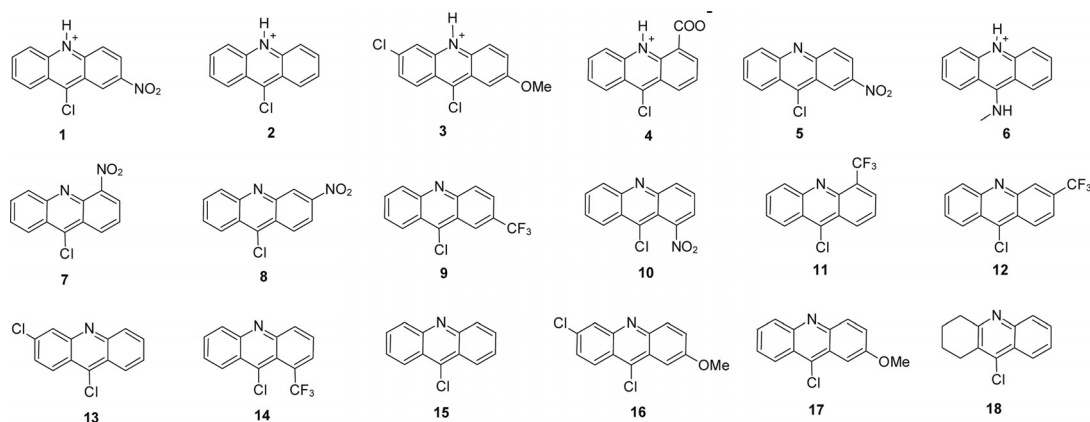

Figure 2. Acridine derivatives investigated computationally.

The H–S–C and S–C–Cl angles in the transition states (Table S2) are quite uniform for all the derivatives, confined to 92–96° and 93–100°, respectively. However, a larger variance is apparent for the bond lengths listed in Table 2. Their correlation with the activation energies is discussed in detail in the next section.

Correlation of the Activation Energies with the Geometry Parameters

The plots of the calculated C–Cl (reactant and TS) and C–S (TS) bond lengths and the reaction energies against the activation energies are shown in Figure 3. A greater number of compounds have been included in this figure with the additional derivatives (**E1**–**E31**, see Table S1 in the Supporting Information) confirming the trends discussed above for **1**–**18**.

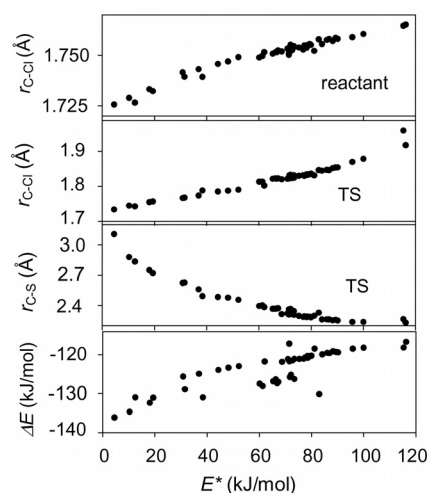Figure 3. Calculated (B3LYP/6-31+G**/CPCM) dependencies of the C–Cl (reactant and TS) and C–S (TS) bond lengths and the reaction energy on the activation energy. Compounds **1**–**18** (Figure 2, without derivative **6**) and **E1**–**E31** (Table S1 in the Supporting Information) are included.

The strong correlation between $E*$ and the C–Cl reactant bond length (Figure 3, top) can be conveniently used to provide a very quick estimation of the activation energy, as the full computation of the transition state is much more computationally demanding than optimization of an equilibrium geometry.

Higher activation energies are clearly associated with longer C–Cl bonds in the TS. A similar correlation was also observed for the relative change in this bond [(d_{TS} – $d_{reactant}$)/$d_{reactant}$, not shown]. This corresponds very well with Hammond's postulate,[12,17] that is, $E*$ is qualitatively proportional to the change in geometry between the reactants and TS.

An opposite correlation is found for the C–S bond formed (Figure 3), that is, it becomes shorter for reactions with higher $E*$. This is also in accordance with Hammond's postulate: There is no C–S bond in the reactants, the shorter the C–S bond the greater the geometrical change between the reactants and TS.

The dependence of ΔE on $E*$ (Figure 3) again corresponds to Hammond's reaction rules and to the concept of product development control,[12] which relates very negative reaction energies to low barriers. In other words, the fast kinetics parallel the relative stabilities of the products. When a TS becomes similar to the product, the activation energy increases.

Experimental Activation Energy for Reaction (2)

Figure 4 shows the dependence of the experimental rate constant for reaction (2) on temperature. Because of the excess of one reactant (BM), its concentration is roughly constant and the reaction behaves like a pseudo-first-order system. The exponential fit corresponding to the Arrhenius formula provides an activation energy of 35 kJ/mol, which is in reasonable agreement with the calculated values listed in Table 2. For compound **3**, derived from **16** by in situ protonation (reaction carried out in AcOH), we calculated a value of 20 kJ/mol, although for a different SH⁻ reagent. Computations with BM were slow and numerically unstable. Nevertheless, the correlation of the calculated results with experiment indicates that the SH⁻ model, in spite of the approximations, is appropriate for qualitatively determining the reaction mechanism and energetics. Note, however, that the experimental value may depend on various parameters that are difficult to take into account theoretically. For example, the relatively slow formation of the acridone byproduct was neglected. The good agreement of the temperature dependence of the rate constant with the theoretical dependence (Arrhenius law, Figure 4) suggests that pseudo-first-order kinetics is appropriate, at least at the beginning of the reaction (up to about 20% conversion).
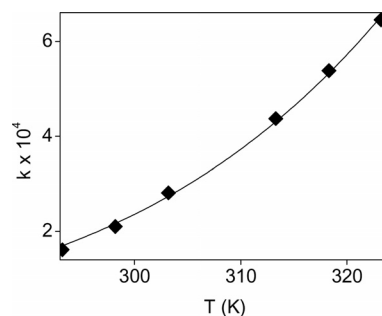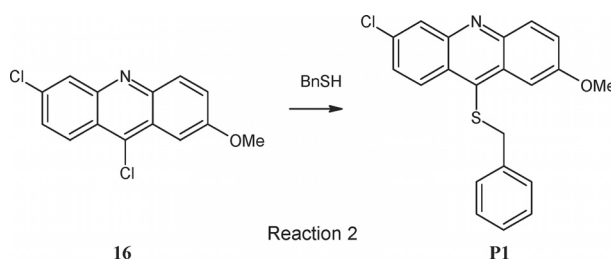

Figure 4. The dependence of the experimental rate constant for reaction (2) on the temperature; an exponential fit is indicated.

Competition Experiment

The reactivities of the compounds decrease in the following order: **12** > **14** > **15** > **16** >> **18**. Reaction half-times for **12**, **14**, and **16** were determined to be approximately 0.5, 1, and 7 h, respectively. Derivative **18** did not react within the timescale of the HPLC monitoring. For **15**, its HPLC signal could not be completely distinguished from the acridone byproduct, nevertheless, we can estimate its reactivity to be higher than that of **16** and lower than that of **14**. The general behavior thus agrees well with the reactivities predicted by the calculations summarized in Table 2. For example, the lowest activation energy (76 kJ/mol) corresponds to the highest reaction rate ($t_{1/2}$ = 0.5 h) for **12**, whereas for **18** the highest activation energy (116 kJ/mol) correlates with the slowest reaction ($t_{1/2}$ >> 24 h).

We also noticed that the reaction yields during the synthesis of compounds **12**, **14**, **15**, and **16** (89, 90, 82, and 65%, respectively) also correlate reasonably well with the theoretical predictions, that is, with increasing activation energies and decreasing reactivities. The yields in real experiments are clearly only weakly related to our abstract theoretical models, nevertheless the correlation confirms the decisive role of the activation energies and the activated complex.

Activation of the Acridine Reactant

According to the computations, most of the acridine substituents, for example, the nitro group and chlorine atom, reduce the activation energy. Only the methoxy group and saturation of the aromatic ring (compound **18**) cause an increase. This is in accordance with described substituent effects for aromatic nucleophilic substitution reactions.[18] The nitro group, for example, is an electron-withdrawing substituent that enhances the reaction. Owing to their negative inductive effects, the chlorine atom and the CF_3 group also increase the reactivity (**9**, **11**–**14**, Figure 1, Table 2), whereas electron-donating substituents (the methoxy group and alkyl chains in partially saturated systems, **16**, **17**, **18**) inhibit the nucleophilic substitution. Note that when both a methoxy group and a chlorine atom are present (**16**), the activation energy is similar to that of bare 9-chloroacridine. The effects of the two substituents cancel each other out.

Although the reaction mechanisms for 4-chloropyridine and 9-chloroacridines are, according to the calculations, almost identical, it should be noted that their reactivities in general are not equivalent. For example, the thermal stability of acridine is lower than that of pyridine.[19]

Modification of the Reaction Mechanism for Quinacrine

Apart from 9-chloroacridine, many aminoacridine derivatives attract attention because of their biological activity. For example, quinacrine is used as a lysosomotropic agent and cysteine protease inhibitor in biochemical applications.[20] On the basis of the calculations (Table 2), we suppose that the rate-determining step (formation of a Meisenheimer complex) found for the chloro derivative is similar also for quinacrine, although some specifics for the amino substituent in the latter have to be taken into account: Quinacrine (pK_a = 10.4)[2a] is more basic than chloroacridine (**16**, pK_a = 6.0).[21] Under physiological conditions (pH = 7.4), quinacrine is completely protonated on N10 and the reaction is accelerated (cf. the activation energies for **16** and **3** are 88 and 20 kJ/mol, respectively). Protonation of the quinacrine derivative is further enhanced by a resonance with the iminium form (**20**, Figure 5).
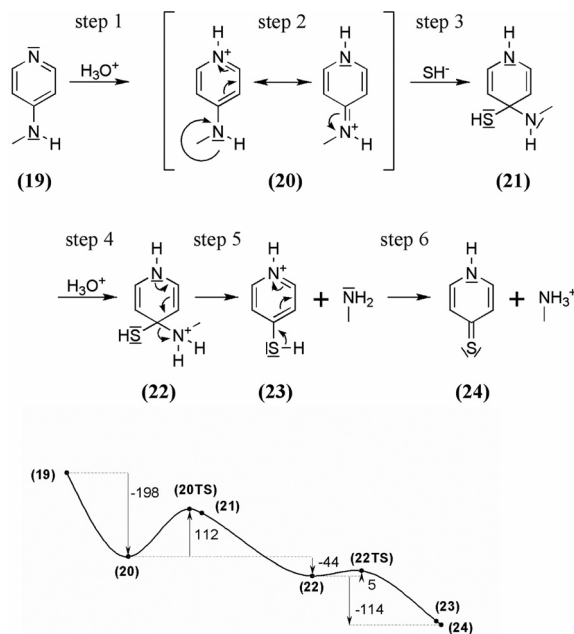

Figure 5. Reaction mechanism for the reaction of 4-methylaminopyridine discussed in the text. Relative energies along the reaction path (bottom, in kJ/mol) of the intermediates were calculated at the B3LYP/6-31+G**/CPCM(H_2O) level of theory.

The reactivity of the quinacrine drug is too complex to be modeled in detail by our computational methods, nevertheless, in Figure 5, we propose a reaction mechanism for a simpler system, 4-methylaminopyridine. Similarly to the chloropyridine, the formation of a Meisenheimer complex (**20TS**) as a transition state is the rate-determining step with an activation energy of 112 kJ/mol. The protonation of the initial amine **19** is associated with a large drop of energy (step 1, Figure 5, ΔE = –198 kJ/mol). A second protonation of amine **21** (step 4) makes the reaction again more energetically viable. CH_3NH_2 is eliminated from **22** with a low reaction barrier (5 kJ/mol). 4-Thiopyridone (**24**) is the final, most energetically-viable product.

Alternative reaction paths were investigated but not found to be reasonable, mostly due to high energy barriers. These included (1) the reaction of SH⁻ with unprotonated 4-methylaminopyridine (**19**), (2) an intramolecular proton transfer in **21** (from SH to NH), and (3) simultaneous methylamine cleavage with thiol group deprotonation.

We are aware that the CPCM solvent model could introduce some errors into the estimated energies, especially those of the proton considered as H_3O^+. Nevertheless, the calculations seem to provide a useful insight into the mechanism. The proton transfer to basic nitrogen atoms (steps 1, 4, and 6, Figure 5) did not exhibit activation barriers. This was verified by the potential energy surface scans performed with the Gaussian suite of programs.[22] Note that at physiological pH, almost all the substrates would already be protonated.

Empirical Rules Derived from the Theoretical Results

We can thus conclude that the computations provide realistic estimates of the relative reactivities of the acridines, which can be used to plan aromatic nucleophilic experiments. Some of the predicted strong correlations between geometry and activation energy are summarized in Table 3. As mentioned above (Figure 3 and Table 2), the dependence of E^* on the reactant geometry is a particularly valuable tool, for example, for future drug design, as it avoids the time-consuming and often laborious TS calculations.

Table 3. Empirical relationships and approximate rules obtained from the reaction path calculations (B3LYP/6-31+G**/CPCM/H_2O) of the acridine derivatives reacting with the HS^- ion.[a]

Unprotonated substrate
$E^* = 3598r_{C-Cl,reactant} - 6234$, $R^2 = 0.98$
$r_{C-Cl,TS} = 6.69r_{C-Cl,reactant} - 9.90$, $R^2 = 0.88$
$r_{C-S,TS} = 837.1r_{C-Cl,reactant}^2 - 2951.4r_{C-Cl,reactant} + 2603.71$, $R^2 = 0.94$
Protonated substrate
$E^* = 2285r_{C-Cl,reactant} - 3939$, $R^2 = 0.95$
$r_{C-Cl,TS} = 3.27r_{C-Cl,reactant} - 3.91$, $R^2 = 0.84$
$r_{C-S,TS} = 1958.4r_{C-Cl,reactant}^2 - 6824.2r_{C-Cl,reactant} + 5947.4$, $R^2 = 0.91$
Additivity effect of the fluorine substitutions on acridine
$E^* = 86.1 - 11.9f_1 - 1.4f_2 - 5.7f_3 - 6.7f_4$, $f_i = 1$ for fluorine at position i, otherwise $f_i = 0$

[a] E^* is in kJ/mol, distances in Å, R^2 is the square of correlation coefficient.

Also, if the TS computation is inevitable, the relation between the reactant and TS geometries can save an enormous amount of computational time. In particular, unrealistic C–Cl and C–S bond lengths in the starting structures typically lead to convergence problems during the reaction path calculation.

In Table 3, relationships for the protonated and unprotonated compounds are given separately. Although the trends are the same, the protonated compounds (E^*, $r_{C-Cl,TS}$) are notably less influenced by the substituents. This can be explained by the strong effect of the hydrogen charge, which dominates other substituent effects in the protonated species.

Substitution at the 1-position of acridine requires particular attention for steric reasons. Bulky substituents with a strong electron-withdrawing effect (NO_2) usually require

high activation energies. Also remarkable is the additivity of the fluorine substitution effect on the activation energy, not observed for the other groups.

Remarks on the Role of the Substituents

The relative influence of substituent positions on the acridine reactivity is summarized in Table 4. In spite of possible computational errors, a more detailed analysis reveals interesting properties of the substituted acridine systems. For example, the OMe group increases the activation energy, but its positive mesomeric (+M) effect is not additive; for the 3,4-dimethoxy derivative the activation energy is lower than for either 3-methoxy or 4-methoxy derivatives. We can explain this by the nonplanar arrangement of aromatic and OMe π-electron systems at the 4-position, which only allows for the negative inductive (–I) effect. This is in agreement with the activation energy of the 2,3-dimethoxy derivative being greater than for either the 2-methoxy or 3-methoxy derivatives, in which the π conjugation is not perturbed. The nitro group displays opposite behavior to OMe, having a strong negative mesomeric effect.

Table 4. Calculated relative influence of substituent positions on reactivity.

Monosubstitution
NO_2: 2 > 4 > 3 > 1
CF_3: 2 > 4 > 3 > 1
Cl: 1 > 4 > 3 > 2
F: 1 > 4 > 3 > 2
OMe: 1 > 3 > 4 > 2
Polysubstitution
F: 1,2,3,4 > 1,3,4 > 1,2,4 > 1,2,3 > 1,4 > 1,3 > 2,3,4 > 1,2 > 3,4 > 1 > 2,4 > 2,3 > 4 > 3 > 2
OMe: 1 > 3,4 > 3 > 4 > 2 > 2,3
Functional groups at a given position
C-1: NO_2 > Cl > F > CF_3 > OMe > H
C-2: NO_2 > CF_3 > Cl > F > H > OMe
C-3: NO_2 > CF_3 > Cl > F > H > OMe
C-4: NO_2 > CF_3 > Cl > F > H > OMe
C-2, C-7: NO_2, NO_2 > NO_2, SO_2H > SO_2H, SO_2H > CHO, CHO > H, H > NH_2, NH_2

The 1-methoxy derivative is more reactive than unsubstituted 9-chloroacridine or the 2-fluoro derivative. This cannot be explained by the decrease in the +M effect of OMe because the OMe group is coplanar with the aromatic system. In this case, the chlorine and oxygen atoms repel each other (Figure 6).
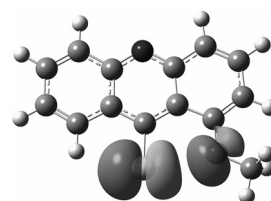

Figure 6. Distortion of the chlorine nonbonding orbital by the presence of the OMe group at the 1-position.

The special character of the 1-position is also apparent for the nitro group. It is not coplanar with the aromatic system, the torsion angle is about 60° for this position, and the –M effect is quite weakened. The activation energy of 1-NO$_2$-acridine is the highest among the nitroacridines. Also, the 4-NO$_2$-acridine is slightly distorted (ca. 30°).

We also see that the activation energy can be most influenced by substituents with a strong mesomeric effect at C2. The activity can be further supported by an attachment of another substituent at C7, equivalent to C2. In this case, the effect is approximately additive.

Although the Mulliken charges calculated for the model reaction of compound **15** (Figure 7) are not directly related to observable properties, they document the large electronic redistribution during the substitution and approximately correlate with the positions of importance for the reactivity. For example, the charge on C3 changes only slightly (–0.04 → –0.08) and this carbon is relatively unimportant. The largest change in charge is on C1, which is clearly very important (cf. Table 4), except for the cases complicated by steric effects. The change in charge is also larger on C4 than on C3, in agreement with their relative influence on reactivity.
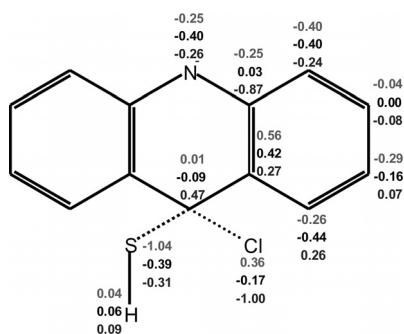

Figure 7. Calculated Mulliken charges of reactants (top), TS (middle), and products (bottom) for the substitution of Cl by SH$^-$ in **15**.

Conclusions

We tested the performance of the computational methods on a reduced pyridine system and roughly estimated their reliability. The similarity in activation energies suggested that the model reproduces the behavior of the more complex acridine derivatives reasonably well. The B3LYP/6-31+G**/CPCM(water) method was then chosen as a compromise between speed and accuracy to investigate the larger systems and to analyze the influence of substituents.

For all acridine derivatives, the energetics and geometry of the activated complex remained qualitatively similar. However, the reaction barrier and thus the actual reactivity could be significantly reduced or increased by substitution of the aromatic systems. In particular, the protonation of the aromatic nitrogen was confirmed to accelerate the reaction.

The experimentally determined activation energy for the model reaction agreed well with these theoretical predic-

tions, as did the relative reactivities determined by the competition experiment.

For the quinacrine drug model, a multistep reaction was suggested that is compliant with physiological conditions. The calculated reaction path indicates that the reaction proceeds through a similar rate-determining step as for the chloro derivative. In addition, unlike the chloro derivative, quinacrine is completely protonated at N10 at physiological pH, which can at least partially explain the high biological activity of this compound.

Finally, we found simple relationships between geometry and reactivity, which can speed up the computational screening of the acridine derivatives. In the future, we hope that the theoretical modeling will be useful in the rational design of acridine aromatic labels, particularly in medicinal chemistry.

Experimental Section

Calculations: In the calculations on reaction (1), acridine was simplified to the pyridine ring. The chlorine atom was attached at C4 of pyridine as a simple leaving group. The reaction path was determined by the QST3[23] method using the Gaussian suite of programs. Activation barriers and reaction energies were estimated at the HF, MP2,[24] B3PW91[25] and B3LYP[25] levels using the 6-31G**, 6-31++G**, and 6-311++G** Gaussian standard Pople-style basis sets. Activation energies were defined as $E^* = E_{TS} - E_A - E_B$, in which TS is the transition state, A is 4-chloropyridine, and B is SH$^-$. Similarly, the reaction energy $\Delta E = E_C + E_D - E_A - E_B$, in which C is pyridine-4-thiol and D is Cl$^-$, was calculated. The solvent environment was accounted for by the CPCM[26] correction. Geometries of the transition states and minima on the potential energy surface were verified by calculation of the harmonic vibrational frequencies. The number of CPCM cavities changes along the reaction coordinate, however, in a model computation, we verified that the energy discontinuity is less than 1 kJ/mol.

The computations of the reaction course were then repeated for a broader range of acridine derivatives **1–18** (Figure 1) using the B3LYP/6-31+G**/CPCM(H$_2$O) level of approximation and, finally, completed with the extended set of compounds **E1–E31** listed in Table S1 in the Supporting Information.

Reactivity Studies: The reaction kinetics were studied for the reaction involving 6,9-dichloro-2-methoxyacridine (**16**, Figure 2) and benzyl mercaptan (BM). Acridine **16** (ca. 2.3 mg) was dissolved in glacial acetic acid (1.6 mL). The mixture was briefly sonicated and then stirred for 10 min to ensure temperature equilibration. BM (ca. 200 µL) was then added. The amounts of all substances were adjusted so the final concentrations were 5.00 mM of **16** and 1.00 M of BM (e.g., 2.335 mg of **16**, 198 µL of BM, and 1.48 mL of acetic acid). After addition of the thiol, the mixture was rigorously stirred for 20 s and then 3 µL of reaction mixture was injected into the HPLC apparatus.

The reaction mixture was analyzed by HPLC at 381 nm with the following solvent gradient: 0 min 40% B, 5 min 66% B, 5.1 min 100% B, 5.7 min 100% B, 5.8 min 40% B. HPLC was in continuous mode (i.e., it was not stopped between analyses) and two subsequent injections were separated by at least 7.3 min, otherwise the peak integrals were inaccurate. The cleanliness of the Hamilton syringe was crucial; after each injection it was rinsed 15 times with THF and 6 times with *t*BuOMe (full volume of the syringe), the

Z. Zawada, J. Šebestík, M. Šafařík, P. Bouř

syringe was dried with dry air for around 20 s, and the piston was wiped dry. The temperature of the syringe and piston was allowed to partially equilibrate with that of the reaction mixture. Before injection, the Hamilton syringe was rinsed three times with the reaction mixture. The time (t) dependence of the product areas (S) was fitted by a first-order kinetic model, $S(t) = S(0) + K[1 - \exp(-kt)]$. By using the Arrhenius relation [$k = A\exp(-E^*/RT)$], the activation energy E^* was calculated from the rate constants (k) obtained at six different temperatures (T) within the interval 293–323 K; R is the universal gas constant and A is a constant independent of temperature.

To obtain information about the dependence of the reaction rate on the substituents and to verify the theoretical predictions, a competition experiment was set up to compare the reactivity of compounds **12**, **14**, **15**, **16**, and **18** (Figure 1) with BM. Each of the five compounds in 2.5 mM acetone solutions (100 μL) were mixed and then BM (2 μL) and acetic acid (500 μL) were added. Pure acetic acid was not used as a solvent for stock solutions because, unlike acetone, it slowly reacts with 9-chloroacridines. After calibration, 5 μL samples were analyzed by HPLC over 24 h so that the relative concentrations of the reactants could be monitored at 239, 247, and 268 nm with the following gradient elution: 0 min 15% B, 1 min 18% B, 2 min 23% B, 3 min 30% B, 4 min 36% B, 12 min 75% B, 12.1 min 100% B. To exclude possible interference by light, the experiment was performed in the dark, although we did not notice any instability in our previous experiments in daylight. BM acts as a radical scavenger and stabilizes potentially light-sensitive acridine chromophores. The relative reactivities were determined according to the time for consumption of the substrates. The reaction was monitored over 24 h.

Chromatographic Procedures: TLC silica gel plates (2 mm) from Merck with F_{254} were employed for preparative TLC, silica gel 60 from Merck was used for column chromatography. HPLC was performed with a ZORBAX Poroshell 120 SB-C18 $3 \times 50\ mm \times 2.7\ \mu m$ column with a flow of 1.00 mL/min at 25.0 °C and gradients obtained from solutions A (0.05% TFA in water) and B (100% ACN). HPLC (199, 220, 270, and 381 nm) was used to determine the purity of compounds using the following gradient: 0 min 15% B, 1 min 18% B, 2 min 23% B, 3 min 30% B, 4 min 36% B, 12 min 75% B, 12.1 min 100% B; purity of all prepared standards >97%.

9-Chloro-3-(trifluoromethyl)acridine (12) and 9-Chloro-1-(trifluoromethyl)acridine (14): The two chloroacridines were prepared according to ref.[27] 3-{[3-(Trifluoromethyl)phenyl]amino}benzoic acid (575 mg, 2 mmol) was dissolved in $POCl_3$ (4 mL) and heated at reflux for 2 h. Excess $POCl_3$ was evaporated. The resulting very viscous liquid was dissolved in ethanol (10 mL). The solution was cooled (dry-ice/ethanol bath) and a concentrated ammonia/water solution (3 mL) was added dropwise. Then the suspension was rigorously stirred for another 20 min in a cooling bath, water was added (40 mL), and the cooling bath removed. The volume was reduced by evaporation to around 10 mL and then extracted with diethyl ether (4×20 mL). The ether fractions were dried with Na_2SO_4 and the solvent was evaporated. The mixture was dissolved in acetone and the products were separated by preparative TLC (DCM/toluene/ethyl acetate, 75:25:5). The products were extracted from silica gel by ethyl acetate. The solvent was evaporated and the residue was extracted with hexane. The hexane was evaporated and the two isomers were obtained in a total yield of 82%.

9-Chloro-3-(trifluoromethyl)acridine (12): Pale-yellow solid, yield 293 mg, 51%. HPLC: t_R = 9.48 min, m.p. 118–120 °C. ^{1}H NMR (400 MHz, $CDCl_3$): δ = 8.47 (m, J = 0.8 Hz, 1 H), 8.46 (dp, J =

9.1, 0.8 Hz, 1 H), 8.36 (ddd, J = 8.8, 1.4, 0.7 Hz, 1 H), 8.16 (ddd, J = 8.8, 1.2, 0.7 Hz, 1 H), 7.79 (ddd, J = 8.8, 6.6, 1.4 Hz, 1 H), 7.68 (dm, J = 9.1 Hz, 1 H), 7.63 (ddd, J = 8.8, 6.6, 1.2 Hz, 1 H) ppm. ^{13}C NMR (101 MHz, $CDCl_3$): δ = 150.0, 147.6, 141.6, 132.2 (q, J = 33.0 Hz), 131.5, 130.3, 128.3 (q, J = 4.7 Hz), 128.2, 126.5, 125.2, 125.2, 124.8, 123.9 (q, J = 272.6 Hz), 122.2 (q, J = 2.9 Hz) ppm. HRMS (EI): calcd. for $C_{14}H_7ClF_3N$ 281.0219 [M]$^+$; found 281.0226.

9-Chloro-1-(trifluoromethyl)acridine (14): Pale-green solid, yield 178 mg, 31%. HPLC: t_R = 8.55 min; m.p. 78–81 °C. ^{1}H NMR (400 MHz, $CDCl_3$): δ = 8.63 (ddd, J = 8.9, 1.3, 0.7 Hz, 1 H), 8.42 (ddq, J = 9.0, 1.2, 0.6 Hz, 1 H), 8.22 (ddd, J = 8.7, 1.2, 0.7 Hz, 1 H), 8.18 (dp, J = 7.3, 1.2 Hz, 1 H), 7.88 (ddd, J = 8.7, 6.6, 1.3 Hz, 1 H), 7.78 (ddq, J = 9.0, 7.3, 0.9 Hz, 1 H), 7.72 (ddd, J = 8.9, 6.6, 1.2 Hz, 1 H) ppm. ^{13}C NMR (101 MHz, $CDCl_3$): δ = 149.8, 148.6, 139.4, 136.3, 131.5, 129.7, 129.3 (q, J = 8.2 Hz), 128.4, 127.8, 126.3, 125.7, 125.1 (q, J = 31.5 Hz), 124.2 (q, J = 273.0 Hz), 121.5 ppm. HRMS (EI): calcd. for $C_{14}H_7ClF_3N$ 281.0219 [M]$^+$; found 281.0212.

General Procedure for the Synthesis of 9-(Benzylsulfanyl)acridines: 9-Chloroacridine (0.4 mmol), BM (110 μL, 0.9 mmol), and NaOH (30 mg, 0.8 mmol) were suspended in a mixture of methanol (1 mL) and THF (0.5 mL). After approximately 2 min of sonication, water (5 mL) and chloroform (5 mL) were added. The organic layer was separated and the water fraction was extracted with chloroform (3×10 mL). The chloroform solution was dried with Na_2SO_4 and the solvent was evaporated. The residue was dissolved in toluene (10 mL) and the solvent was evaporated. This procedure was repeated three times. The crude product was purified by chromatography (column or TLC).

9-(Benzylsulfanyl)-3-(trifluoromethyl)acridine: 9-Chloro-3-(trifluoromethyl)acridine (**12**) (112 mg, 0.4 mmol) was used. The crude product was purified by preparative TLC (hexane/acetone, 90:10) to yield 131 mg (89%) of a pale-yellow solid. HPLC: t_R = 11.17 min; m.p. 92–94 °C. ^{1}H NMR (400 MHz, $CDCl_3$): δ = 8.67 (dp, J = 9.1, 0.9 Hz, 1 H), 8.61 (ddd, J = 8.8, 1.4, 0.7 Hz, 1 H), 8.46 (m, J = 1.8, 0.9 Hz, 1 H), 8.16 (ddd, J = 8.8, 1.3, 0.7 Hz, 1 H), 7.74 (ddd, J = 8.8, 6.6, 1.4 Hz, 1 H), 7.55 (ddq, J = 9.1, 1.8, 0.4 Hz, 1 H), 7.53 (ddd, J = 8.8, 6.6, 1.3 Hz, 1 H), 7.03–6.93 (m, 3 H), 6.79 (m, 2 H), 3.99 (s, 2 H) ppm. ^{13}C NMR (101 MHz, $CDCl_3$): δ = 149.7, 147.4, 142.7, 137.0, 131.64 (q, J = 32.7 Hz), 131.0, 130.5, 130.2, 130.1, 128.8, 128.6, 128.5, 128.4 (q, J = 4.7 Hz), 127.8, 127.6, 126.9, 124.0 (q, J = 272.5 Hz), 121.6 (q, J = 2.9 Hz), 42.1 ppm. IR (CHCl$_3$): $\tilde{\nu}$ = 1328 (vs, CF$_3$), 2931 (w, CH$_2$) cm^{-1}. HRMS (EI): calcd. for $C_{21}H_{14}F_3NS$ 369.0799 [M]$^+$; found 369.0800.

9-(Benzylsulfanyl)-1-(trifluoromethyl)acridine: 9-Chloro-1-(trifluoromethyl)acridine (**14**) (112 mg, 0.4 mmol) was used. The crude product was purified by preparative TLC (hexane/acetone, 90:10) to yield 133 mg (90%) of a yellow solid. HPLC: t_R = 9.30 min; m.p. 104–107 °C. ^{1}H NMR (400 MHz, $CDCl_3$): δ = 8.84 (ddd, J = 8.8, 1.3, 0.7 Hz, 1 H), 8.19 (ddq, J = 8.6, 1.3, 0.5 Hz, 1 H), 8.13 (ddd, J = 8.7, 1.2, 0.7 Hz, 1 H), 7.91 (ddq, J = 7.2, 1.3, 0.7 Hz, 1 H), 7.76 (ddd, J = 8.7, 6.6, 1.3 Hz, 1 H), 7.61 (ddd, J = 8.8, 6.6, 1.2 Hz, 1 H), 7.59 (ddq, J = 8.6, 7.2, 0.9 Hz, 1 H), 6.88–6.77 (m, 3 H), 6.48 (m, 2 H), 3.69 (s, 2 H) ppm. ^{13}C NMR (101 MHz, $CDCl_3$): δ = 148.6, 148.6, 143.0, 136.4, 135.6, 131.0, 130.4, 130.0, 129.2 (q, J = 7.2 Hz), 128.5, 128.0, 127.9, 127.8, 127.4, 127.1, 127.0, 126.5 (q, J = 31.2 Hz), 124.7 (q, J = 272.8 Hz), 43.1 ppm. IR (CHCl$_3$): $\tilde{\nu}$ = 1288 (vs, CF$_3$), 2930 (w, CH$_2$) cm^{-1}. HRMS (EI): calcd. for $C_{21}H_{14}F_3NS$ 369.0799 [M]$^+$; found 369.0798.

9-(Benzylsulfanyl)acridine: 9-Chloroacridine (**15**) (89 mg, 0.4 mmol) was used. The crude product was purified by preparative TLC (hex-

ane/ethyl acetate, 80:20) to yield 103 mg (82%) of a pale-yellow solid. HPLC: t_R = 5.55 min; m.p. 103–106 °C. ^{1}H NMR (400 MHz, CDCl$_3$): δ = 8.59 (ddd, J = 8.8, 1.4, 0.7 Hz, 2 H), 8.14 (ddd, J = 8.7, 1.2, 0.7 Hz, 2 H), 7.68 (ddd, J = 8.7, 6.6, 1.4 Hz, 2 H), 7.45 (ddd, J = 8.8, 6.6, 1.2 Hz, 2 H), 7.03–6.94 (m, 3 H), 6.87–6.82 (m, 2 H), 3.98 (s, 2 H) ppm. ^{13}C NMR (101 MHz, CDCl$_3$): δ = 148.9, 142.1, 137.3, 130.2, 130.2, 129.3, 128.8, 128.43, 127.4, 126.9, 126.7, 41.9 ppm. HRMS (EI): calcd. for $C_{20}H_{15}NS$ 301.0925 [M]$^+$; found 301.0922.

9-(Benzylsulfanyl)-6-chloro-2-methoxyacridine: 6,9-Dichloro-2-methoxyacridine (**16**) (114 mg, 0.4 mmol) was used. The crude product was purified by column chromatography (first chloroform 100%, then chloroform/methanol, 92:8) to yield 97 mg (65%) of an orange solid. HPLC: t_R = 9.61 min; m.p. 153–155 °C. ^{1}H NMR (400 MHz, CDCl$_3$): δ = 8.47 (dd, J = 9.3, 0.4 Hz, 1 H), 8.10 (dd, J = 2.1, 0.4 Hz, 1 H), 7.98 (dd, J = 9.4, 0.4 Hz, 1 H), 7.66 (dd, J = 2.8, 0.4 Hz, 1 H), 7.36 (m, 2 H), 7.05–6.93 (m, 3 H), 6.78 (m, 2 H), 3.94 (s, 2 H), 3.83 (s, 3 H) ppm. ^{13}C NMR (101 MHz, CDCl$_3$): δ = 158.3, 147.1, 146.6, 139.0, 137.4, 135.0, 131.7, 130.8, 128.8, 128.5, 128.5, 128.0, 127.9, 127.5, 126.1, 102.3, 55.7, 41.4 ppm. HRMS (EI): calcd. for $C_{21}H_{16}NOSCl$ 365.0641; found 365.0643.

Supporting Information (see footnote on the first page of this article): Experimental and computational details, compound characterizations, computations for other acridine derivatives.

[1] J. Chiron, J. P. Galy, *SynLett* **2003**, *15*, 2349–2350.
[2] a) J. Šebestík, J. Hlaváček, I. Stibor, *Curr. Protein Pept. Sci.* **2007**, *8*, 471–483; b) M. Demeunynck, F. Charmantray, A. Martelli, *Curr. Pharm. Des.* **2001**, *7*, 1703–1724; c) S. Claude, J. M. Lehn, J. P. Vigneron, *Tetrahedron Lett.* **1989**, *30*, 941–944; d) Z. Zawada, J. Šebestík, M. Šafařík, A. Krejčířiková, A. Březinová, J. Hlaváček, I. Stibor, K. Holada, P. Bouř, in: *Peptides 2010* (Eds.: M. Lebl, M. Meldal, K. Jensen, T. Hoeg-Jensen), Proceedings of the 31st European Peptide Symposium, European Peptide Society, Copenhagen, **2010**, pp. 84–85.
[3] J. Šebestík, I. Stibor, K. Hlaváček, *J. Pept. Sci.* **2006**, *12*, 472–480.
[4] a) D. J. Wallace, *Semin. Arthritis Rheum.* **1989**, *18*, 282–297; b) C. Korth, B. C. H. May, F. E. Cohen, S. B. Prusiner, *Proc. Natl. Acad. Sci. USA* **2001**, *98*, 9836–9841; c) B. C. H. May, A. T. Fafarman, S. B. Hong, M. Rogers, L. W. Deady, S. B. Prusiner, F. E. Cohen, *Proc. Natl. Acad. Sci. USA* **2003**, *100*, 3416–3421.
[5] I. Lasnitzki, J. H. Wilkinson, *Br. J. Cancer* **1948**, *2*, 369–375.
[6] a) R. L. Krauth-Siegel, H. Bauer, H. Schirmer, *Angew. Chem.* **2005**, *117*, 698; *Angew. Chem. Int. Ed.* **2005**, *44*, 690–715; b) A. Saravanamuthu, T. J. Vickers, C. S. Bond, M. R. Peterson, W. N. Hunter, A. H. Fairlamb, *J. Biol. Chem.* **2004**, *279*, 29493–29500; c) F. Wild, J. M. Young, *J. Chem. Soc.* **1965**, 7261–7274; d) J. C. Burnett, J. J. Schmidt, R. G. Stafford, R. G. Panchal, T. L. Nguyen, A. R. Hermone, J. L. Vennerstrom, C. F. McGrath, D. J. Lane, E. A. Sausville, D. W. Zaharevitz, R. Gussio, S. Bavari, *Biochem. Biophys. Res. Commun.* **2003**, *310*, 84–93.
[7] P. Spilman, P. Lessard, M. Sattavat, C. Bush, T. Tousseyn, E. J. Huang, K. Giles, T. Golde, P. Das, A. Fauq, S. B. Prusiner, S. J. DeArmond, *Proc. Natl. Acad. Sci. USA* **2008**, *105*, 10595–10600.
[8] a) J. K. Marquis, *Biochem. Pharmacol.* **1990**, *40*, 1071–1076; b) S. E. Freeman, R. M. Dawson, *Prog. Neurobiol.* **1991**, *36*, 257–277.
[9] B. R. Brown, W. J. Firth, L. W. Yielding, *Mutat. Res.* **1980**, *72*, 373–388.
[10] D. J. A. Bridewell, G. J. Finlay, B. C. Baguley, *Anti-Cancer Drug Des.* **2001**, *16*, 317–324.
[11] J. Šebestík, M. Šafařík, I. Stibor, J. Hlaváček, *Biopolymers* **2006**, *84*, 605–614.
[12] R. Bruckner, *Advanced Organic Chemistry: Reaction Mechanisms*, Springer, New York, **2002**.
[13] a) A. Paul, S. Ladame, *Org. Lett.* **2009**, *11*, 4894–4897; b) M. Weltrowski, A. Ledochowski, P. Sowinski, *Pol. J. Chem.* **1982**, *56*, 77–82.
[14] a) A. Kunikowski, A. Ledochowski, *Pol. J. Chem.* **1981**, *55*, 1979–1984; b) C. M. Johnson, T. W. Linsky, W. D. Yoon, M. D. Person, W. Fast, *J. Am. Chem. Soc.* **2011**, *133*, 1553–1562.
[15] a) J. R. Goodell, B. Svensson, D. M. Ferguson, *J. Chem. Inf. Model.* **2006**, *46*, 876–883; b) A. Wrooblewska, J. Meszko, K. Krzyminsky, Y. Ebead, J. Blazejowski, *Chem. Phys.* **2004**, *303*, 301–308.
[16] a) L. M. Herrmann, B. Caughey, *Neuroreport* **1998**, *9*, 2457–2461; b) J. I. Shin, J. Y. Shin, J. S. Kim, Y. S. Yang, Y. K. Shin, D. H. Kweon, *Biochem. Biophys. Res. Commun.* **2008**, *377*, 995–1000; c) J. Y. Shin, J. I. Shin, J. S. Kim, Y. S. Yang, Y. K. Shin, K. K. Kim, S. Lee, D. H. Kweon, *Mol. Cells* **2009**, *27*, 673–680.
[17] G. S. Hammond, *J. Am. Chem. Soc.* **1955**, *77*, 334–338.
[18] M. B. Smith, J. March, *March's Advanced Organic Chemistry*, 5th ed., Wiley, New York, **2001**.
[19] A. R. Katritzky, R. A. Barcock, M. Siskin, W. N. Olmstead, *Energy Fuels* **1994**, *8*, 990–1001.
[20] K. Doh-Ura, T. Iwaki, B. Caughey, *J. Virol.* **2000**, *74*, 4894–4897.
[21] M. G. Ferlin, C. Marzano, G. Chiarelotto, F. Baccichetti, F. Bordin, *Eur. J. Med. Chem.* **2000**, *35*, 827–837.
[22] M. J. Frisch, G. W. Trucks, H. B. Schlegel, G. E. Scuseria, M. A. Robb, J. R. Cheeseman, G. Scalmani, V. Barone, B. Mennucci, G. A. Petersson, H. Nakatsuji, M. Caricato, X. Li, H. P. Hratchian, A. F. Izmaylov, J. Bloino, G. Zheng, J. L. Sonnenberg, M. Hada, M. Ehara, K. Toyota, R. Fukuda, J. Hasegawa, M. Ishida, T. Nakajima, Y. Honda, O. Kitao, H. Nakai, T. Vreven, J. A. Montgomery Jr., J. E. Peralta, F. Ogliaro, M. Bearpark, J. J. Heyd, E. Brothers, K. N. Kudin, V. N. Staroverov, R. Kobayashi, J. Normand, K. Raghavachari, A. Rendell, J. C. Burant, S. S. Iyengar, J. Tomasi, M. Cossi, N. Rega, J. M. Millam, M. Klene, J. E. Knox, J. B. Cross, V. Bakken, C. Adamo, J. Jaramillo, R. Gomperts, R. E. Stratmann, O. Yazyev, A. J. Austin, R. Cammi, C. Pomelli, J. W. Ochterski, R. L. Martin, K. Morokuma, V. G. Zakrzewski, G. A. Voth, P. Salvador, J. J. Dannenberg, S. Dapprich, A. D. Daniels, O. Farkas, J. B. Foresman, J. V. Ortiz, J. Cioslowski, D. J. Fox, *Gaussian 09*, Revision A.02, Gaussian, Inc., Wallingford, CT, **2009**.
[23] C. Peng, P. Y. Ayala, H. B. Schlegel, M. J. Frisch, *J. Comput. Chem.* **1996**, *17*, 49–56.
[24] C. Møller, M. S. Plesset, *Phys. Rev.* **1934**, *46*, 618–622.
[25] A. D. Becke, *J. Chem. Phys.* **1993**, *98*, 5648–5652.
[26] a) A. Klamt, in: *The Encyclopedia of Computational Chemistry*, vol. 1 (Eds.: P. v. Ragué Schleyer, N. L. Allinger, T. Clark, J. Gasteiger, P. A. Kollman, H. F. Schaefer III, P. R. Schreiner), Wiley, Chichester, **1998**, pp. 604–615; b) E. Cances, B. Mennucci, J. Tomasi, *J. Chem. Phys.* **1997**, *107*, 3032–3041.
[27] J. H. Wilkinson, I. L. Finar, *J. Chem. Soc.* **1948**, 32–35.